Weak Chaos and the "Melting Transition" in a Confined Microplasma System

Chris Antonopoulos[1], Vasileios Basios[1] and Tassos Bountis[2]

December 15, 2009

[1]Interdisciplinary Center for Nonlinear Phenomena and Complex Systems (CeNoLi), Service de Physique des Systèmes Complexes et Mécanique Statistique,
Université Libre de Bruxelles, 1050, Brussels, Belgium

[2]Center for Research and Applications of Nonlinear Systems (CRANS), Department of Mathematics,
University of Patras, 26500, Patras, Greece

Abstract

We present results demonstrating the occurrence of changes in the collective dynamics of a Hamiltonian system which describes a confined microplasma characterized by long–range Coulomb interactions. In its lower energy regime, we first detect macroscopically, the transition from a "crystalline–like" to a "liquid–like" behavior, which we call the "melting transition". We then proceed to study this transition using a microscopic chaos indicator called the *Smaller Alignment Index* (SALI), which utilizes two deviation vectors in the tangent dynamics of the flow and is nearly constant for ordered (quasi–periodic) orbits, while it decays exponentially to zero for chaotic orbits as $\exp(-(\lambda_1 - \lambda_2)t)$, where $\lambda_1 > \lambda_2 > 0$ are the two largest Lyapunov exponents. During the "melting phase", SALI exhibits a peculiar, stair–like decay to zero, reminiscent of "sticky" orbits of Hamiltonian systems near the boundaries of resonance islands. This alerts us to the importance of the $\Delta\lambda = \lambda_1 - \lambda_2$ variations in that regime and helps us identify the energy range over which "melting" occurs as a multi–stage diffusion process through weakly chaotic layers in the phase space of the microplasma. Additional evidence supporting further the above findings is given by examining the $GALI_k$ indices, which generalize SALI ($=GALI_2$) to the case of $k > 2$ deviation vectors and depend on the complete spectrum of Lyapunov exponents of the tangent flow about the reference orbit.

1 Introduction

It has long been established that microscopic deterministic chaos provides an efficient mechanism for the mixing of orbits in the phase–space of dynamical systems, leading to the decay of statistical correlations as time evolves. Thus, chaotic dynamics can magnify small scale fluctuations and justify the existence

of macroscopic variables like entropy and temperature, which are of central importance in an analysis based on non–equilibrium statistical mechanics [21].

The main purpose of the work presented here is to study the "melting transition" in a microplasma model, using standard methods, as well as certain recently–developed techniques for chaos detection, such as the *Smaller Alignment Index* (SALI) [35, 37, 38] and its extension to the so–called *Generalized Alignment Index* (GALI) [39, 36, 1]. This latter approach is based on geometrical aspects of the microscopic dynamics and has significant computational advantages over more classical indicators based either on local dynamics, such as the Lyapunov exponents, or statistical properties, such as the mean temperature or the Kolmogorov–Sinai entropy. In fact, the use of these novel indices often constitutes an improvement of several orders of magnitude in CPU and dynamical time for the identification of the chaotic or ordered nature of single orbits [11, 35, 37, 38, 36, 3, 2, 1].

The utility of SALI (or GALI) methods in detecting dynamical regime changes in few–particle Hamiltonian systems [36] is due to their sensitivity in tracing out the geometrical properties of the tangent dynamics of the flow. Thus, they provide accurate information about regime changes when important parameters of the system are varied. For example, the existence of "sticky" regions and the occurrence of slow diffusion in weakly chaotic domains is detectable and the distinction between order and strongly chaotic motion is easily made by these methods [36]. In the case of fully developed chaotic motion, SALI is particularly efficient, since it decays exponentially as $\exp(-(\lambda_1 - \lambda_2)t)$ where $\lambda_1 > \lambda_2 > 0$ are the two largest Lyapunov exponents [38], while for ordered orbits SALI $\propto$ const.> 0.

The system we consider here consists of N interacting particles described by a Hamiltonian function of the form

$$H(\vec{q}, \vec{p}) = K(\vec{p}) + V(\vec{q})$$

where the kinetic energy part $K(\vec{p}) = \frac{1}{2}\sum_{i=1}^{N} p_i^2$ is quadratic in the generalized momenta $\vec{p} = (p_1, \ldots, p_N)$ and the potential energy $V(\vec{q})$ is a function of its generalized position coordinates $\vec{q} = (q_1, \ldots, q_N)$. In the case of confined systems, one takes V as the sum of two terms: $V(\vec{q}) = V_{tr}(\vec{q}) + V_{in}(\vec{q})$, where $V_{tr}(\vec{q})$ represents the potential of the trap (being a smooth positive function), while $V_{in}(\vec{q})$ accounts for the interactions amongst the N particles. The fact that N is a finite number classifies the system as "small", in contrast to a "large" thermodynamic system (where one lets N and the volume V tend to infinity in such a way that N/V is a finite real constant) [24, 23].

Small, finite Hamiltonian systems in contrast to large, infinite, systems do not exhibit phase transitions in the standard sense. The characteristic discontinuities or singularities in thermodynamic functions or their derivatives, which is the signature of a phase transition in large systems would now appear as steep but continuous changes in their thermodynamic functions or their derivatives [24].

Phase transitions in small systems, have also been associated, quite recently, with certain topology changes in configuration space [17, 16]. These developments are stemming from earlier work on Hamiltonian systems exhibiting chaotic instabilities associated with singular behaviour of their configuration–space curvature fluctuations at their phase transition point [14, 15, 29]. Furthermore, investigations of the temperature dependence of the largest Lyapunov

exponent and other observables related to the "topological hypothesis" and the issue of phase transitions in many–degrees of freedom systems is thoroughly presented in [16] and references therein.

In this paper, our model Hamiltonian system describes a microplasma characterized by long range (non shielded) Coulomb interactions described by the potential $V_{in}(\vec{q})$. The microplasma is confined in a Penning trap given by the potential $V_{tr}(\vec{q})$ and our aim is to study the motion of its ions as the energy increases. The system evolves, in general, in 3 spatial dimensions and contains a relatively small number of ions for which the tracking of individual trajectories is numerically as well as experimentally feasible [34, 26, 10, 13, 33, 25].

It is important to note that Lyapunov exponents have already been used to investigate spatially extended plasmas [5, 4, 42] as well as 1–dimensional wave–particle plasma models [20, 27]. Moreover, as Gaspard [22] has demonstrated, for a realistic Hamiltonian model in 3 spatial dimensions containing a relatively small number of ions, the long range nature of the Coulomb interaction $V_{in}(\vec{q})$ makes the maximum Lyapunov exponents behave differently in microplasmas than in many–particle systems with short–range interactions, such as a hard–ball fluid or systems with shielded ionic interactions (Yukawa potentials). A detailed analysis of the differences between shielded (Yukawa–like) and unshielded Coulomb potentials can be found in the book by Baus and Tejero [6]. Indeed, in microplasmas composed of more than a few dozen of ions, the behavior of the maximum Lyapunov exponent, especially in the "gas phase", was explained following purely statistical mechanics arguments [22].

The plan of the paper is the following: The Hamiltonian representation of our system and a summary of previous work are presented in Sec. 2. Some background material related to the SALI method and the spectrum of Lyapunov exponents are given in Sec. 3. The calculation of Lyapunov exponents spectra for our system is presented in Sec. 4, while the detection of the "melting transition" as a passage from weak to strong chaos is demonstrated in Sec. 5. Finally, our conclusions are presented in Sec. 6.

2 Description of the model and summary of previous work

Let us consider a microplasma of N ions of equal mass $m = 1$ and electric charge q in a Penning trap with electrostatic potential

$$\Phi(x, y, z) = V_0 \frac{2z^2 - x^2 - y^2}{r_0^2 + 2z_0^2} \tag{1}$$

and constant magnetic field along the z direction with a vector potential of the form

$$\mathbf{A}(x, y, z) = \frac{1}{2}(-By, Bx, 0). \tag{2}$$

Then, the Hamiltonian of the full system is given by

$$\mathcal{H} = \sum_{i=1}^{N} \left\{ \frac{1}{2m}(\mathbf{p}_i - q\mathbf{A}(\mathbf{r}_i))^2) + q\Phi(\mathbf{r}_i) \right\} + \sum_{1 \le i < j \le N} \frac{q^2}{4\pi\epsilon_0 r_{ij}} \tag{3}$$

where $\mathbf{r_i}$ is the position of the ith ion, r_{ij} is the Euclidean distance between the ith and jth ions and ϵ_0 is the vacuum permittivity. In the Penning trap, the ions are subjected to a harmonic confinement in the z direction with frequency

$$\omega_z = \sqrt{\frac{4qV_0}{m(r_0^2 + 2z_0^2)}} \tag{4}$$

while in the perpendicular direction (due to the cyclotron motion) they rotate with frequency $\omega_c = qB/m$. Thus, in a frame rotating around the z axis at the Larmor frequency $\omega_L = \omega_c/2$, the ions feel a harmonic confinement of frequency $\omega_x = \omega_y = \sqrt{\frac{\omega_c^2}{4} - \frac{\omega_z^2}{2}}$ in the direction perpendicular to the magnetic field. In the rescaled time $\tau = \omega_c t$, position $\mathbf{R} = \mathbf{r}/a$ and energy $H = \frac{\mathcal{H}}{m\omega_c^2 a^2}$ with $a = \left(\frac{q^2}{4\pi\epsilon_0 m\omega_c^2}\right)^{\frac{1}{3}}$, the Hamiltonian (3) describing the motion takes the form

$$H = \sum_{i=1}^{N}\Big[\frac{1}{2}\mathbf{P}_i^2\Big] + \sum_{i=1}^{N}\Big[\Big(\frac{1}{8} - \frac{\gamma^2}{4}\Big)(X_i^2 + Y_i^2) + \frac{\gamma^2}{2}Z_i^2\Big] + \sum_{i<j}\frac{1}{R_{ij}} = E \tag{5}$$

where E is the total energy of the system, $\mathbf{R}_i = (X_i, Y_i, Z_i)$ and $\mathbf{P}_i = (P_{X_i}, P_{Y_i}, P_{Z_i})$ are the positions and canonically conjugate momenta respectively, R_{ij} is the Euclidean distance between different ions i, j given by

$$R_{ij} = \sqrt{(X_i - X_j)^2 + (Y_i - Y_j)^2 + (Z_i - Z_j)^2} \tag{6}$$

and $\gamma = \omega_z/\omega_c$.

The ions are trapped in bounded motion under the condition that

$$0 < |\gamma| < \frac{1}{\sqrt{2}}. \tag{7}$$

The trap is called prolate if $0 < |\gamma| < \frac{1}{\sqrt{6}}$, isotropic if $|\gamma| = \frac{1}{\sqrt{6}}$ and oblate if $\frac{1}{\sqrt{6}} < |\gamma| < \frac{1}{\sqrt{2}}$. So, the motion is quasi 1–dimensional in the limit $\gamma \to 0$ and quasi 2–dimensional in the limit $\gamma \to 1/\sqrt{2}$. The Z direction is a symmetry axis and hence the Z component of the angular momentum $L_Z = \sum_{i=1}^{N} X_i P_{Y_i} - Y_i P_{X_i}$ is conserved, being thus, a second integral of the motion. We suppose from now on that the angular momentum is equal to zero (i.e. $L_Z = 0$) and that the motion is studied in the Larmor rotating frame.

In [22], it was shown that the motion of the ions governed by Hamiltonian (5) is generally very sensitive to initial conditions and has at least one positive maximum Lyapunov exponent, while a first study of its dependence on the energy, number of ions and trap geometry was also presented. At low kinetic energies, where the microplasma forms an ion crystal, chaos is considerably reduced, since the motion is quasi–harmonic around stable equilibrium configurations. On the other hand, at high temperatures (or kinetic energies), the maximum Lyapunov exponent decreases, as Coulomb interactions become negligible and the microplasma forms a thermal cloud of nearly independent ions moving throughout the full extent of the harmonic potential of the trap. Finally, for intermediate values of the energy, there is a regime of chaotic behavior which becomes wider as the number of ions increases. It is in this regime that

the maximum Lyapunov exponent attains a peak, whose value increases as a function of the number of ions.

A crucial aspect related to our work is that of the geometry of the trap. As has been demonstrated in [22] for prolate traps the maximum Lyapunov exponent (and therefore the K-S entropy of the system) show a distinctively smoother increase in comparison to the oblate traps in the energy values interval from E_{min} (its minimum) to E_0 (its maximum). The transition of interest for our analysis is taking place within a small interval of energies at the beginning, i.e. just after E_{min}. Therefore, the slower the increase of the function $E = E(H)$ the higher the resolution required and the more accurate (and time–consuming) the numerical computation needed. Of course, if one argues in analogy to the standard phase transition theory, the dimensionality of the problem makes it easier to detect transitions in two or three spatial dimensions. But systems with long range interactions may still exhibit a transition even in one dimension. This justifies the choice of small γ adopted in the present paper as being both physically challenging and numerically tractable.

2.1 Crossover through different dynamical regimes

At zero temperature, the system freezes at a crystalline state (see [22] and in particular refs. [20] – [25] therein) reminiscent of Wigner crystals [44]. In that case, the ion crystal is composed of several concentric rings for the case of an oblate (quasi 2–dimensional) trap or a single line of ions in the case of a prolate (quasi 1–dimensional) trap. As temperature rises slightly above zero, the ions execute quasi–periodic motion about stable periodic orbits moving around their equilibrium position. This is the regime where stable normal modes of vibration play an important role, as expected.

At slightly higher temperatures, the system "bifurcates" from the regime of quasi–harmonic motion to one where it executes quasiperiodic motion in the form of a collective soft-mode. We use the term "soft-mode" here since the dynamics is similar to what would be expected under a collective force on the particles, which diminishes as the energy increases. The frequencies of the normal vibrational modes become smaller and smaller and tend to zero at the transition.

As the energy continues to increase, these soft modes overcome the energy barriers and set out to explore broader domains of phase space. At even higher temperatures, their motion becomes erratic and the ion crystal "melts", entering a regime of strongly chaotic motion in phase space.

As the temperature increases further, the ions form a thermal cloud in which the mean Coulomb potential energy starts to become negligible with respect to the mean kinetic energy and mean harmonic potential energy. It has been shown that the maximum Lyapunov exponent λ_1 reaches its peak value at energies well above the "melting phase", while this transition is not manifested in the behavior of the Lyapunov exponents as a function of the number of particles N or the energy E.

Finally, for energies beyond the peak value of the maximum Lyapunov exponent, the motion is dominated by the kinetic energy part and the system becomes amenable to a statistical mechanical treatment with considerable accuracy, in spite of the small number of particles present. Indeed, at such high temperatures T, the spatial disorder of the microplasma can be described in

terms of its thermodynamic entropy and its maximum Lyapunov exponent λ_1 expressed by the theoretical estimate [22]

$$\lambda_1 \sim \left\langle \frac{N^2}{R_{ij}} \right\rangle^{\frac{1}{2}} \sim N \frac{(\ln T)^{\frac{1}{2}}}{T^{\frac{3}{4}}} \text{ for } T \to \infty \tag{8}$$

which may be used to characterize the crossover to the regime of thermal cloud motion, albeit at a high computational cost for the determination of λ_1.

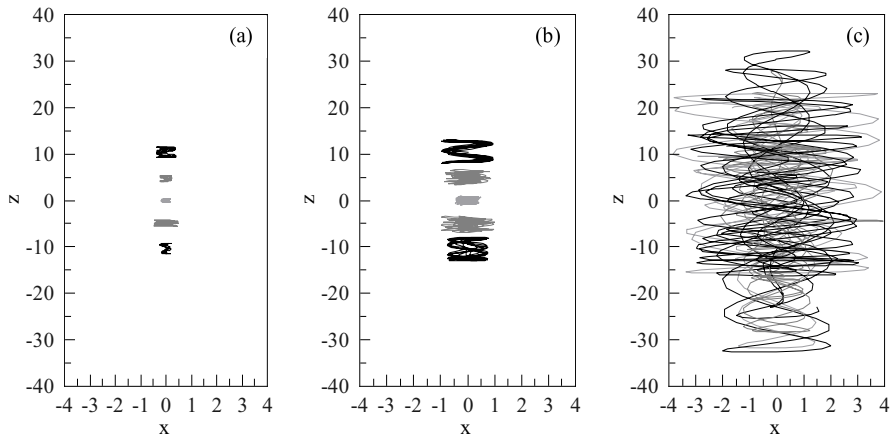

Figure 1: Plot of typical orbits for $N = 5$ and $\gamma = 0.07$ (prolate quasi 1–dimensional geometry): (a) At $E = 2$ the motion is dominated by its stable normal modes and "crystalline" behavior is observed. (b) At $E = 2.35$ a transition to chaotic motion occurs, where "melting" is expected to take place. (c) At $E = 9$ the onset of "thermal cloud" behavior is evident.

Furthermore, in [22], the maximum value of λ_1 is numerically observed to obey a power law with respect to the energy as well as the number of ions. Thus, one reaches the conclusion that, for a prolate trap geometry (quasi 1–dimensional), the "melting transition" and its associated microscopic dynamical behavior should be detectable at low energies and few number of ions (e.g. for $N = 5$ and $\gamma = 0.07$).

The different characteristic kinds of motion in such a setting are depicted in Fig. 1. Panel (a) presents a typical behavior of the ions at energy $E = 2$, where the dynamics is dominated by stable normal modes that correspond to "crystalline" behavior. At the slightly increased energy $E = 2.35$ of panel (b) we observe the occurrence of a transition from stable collective (quasi–periodic) motion to chaotic behavior. Finally, in panel (c), the onset of a fully "thermal" cloud behavior is apparent at the energy $E = 9$. So, for the rest of the paper we consider the case of $N = 5$ ions in the prolate trap geometry with $\gamma = 0.07$.

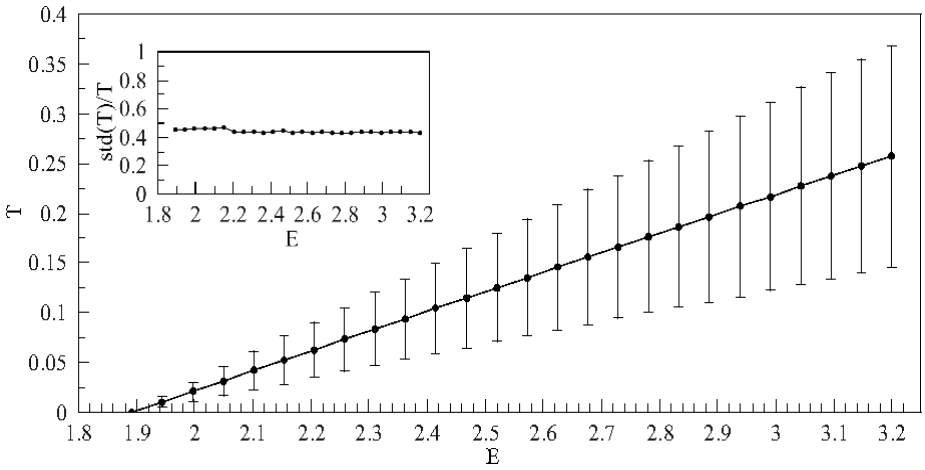

Figure 2: Plot of the dependence of the temperature T (as in eq. (9), dimensionless scale) on the energy E for the microplasma system (5) of $N = 5$ ions in a prolate Penning trap ($\gamma = 0.07$). The error bars represent one standard deviation from the time averaged temperature T. Clearly, the crossover from ordered to weakly chaotic motion around $E \in (2, 2.5)$ does not occur in a manner justifying the use of statistical mechanics considerations. In the inset, the ratio of the standard deviation of the time averaged T to the time averaged temperature T shows that they are comparable.

The temperature, in dimensionless units,

$$T \propto v_{rms}^2 = \left\langle \|\mathbf{P}\|^2 \right\rangle_N \equiv \frac{1}{N} \sum_{i=1}^{N} \|\mathbf{P}_i\|^2 \tag{9}$$

(where $\|\mathbf{P}_i\|$ denotes the Euclidean norm of the ith ions' velocity $\mathbf{P}_i$) averaged over the time t which is a proportional quantity of the mean kinetic energy of the ions is plotted in Fig. 2, as a function of the energy E for the microplasma (5) with $N = 5$ ions in the prolate Penning trap with $\gamma = 0.07$. Evidently, the melting of the crystal here is not associated with a sharp increase of T at some critical energy, as would be expected from a first order phase transition. Note also in Fig. 2 that the fluctuations of T (measured by its standard deviation) cannot provide a clear indication of the crossover from a regime of stable oscillations, through "melting", to strongly developed chaotic motion. So, the use of statistical mechanics considerations must focus on the importance of large fluctuations. Indeed, the inset of Fig. 2 shows that the fluctuations of the time averaged temperature T, in the crossover regime, are comparable with the values of the time averaged temperature itself.

One can, therefore, say that there is no "macroscopic" methodology for detecting dynamical regime changes in system (5) that might be useful to theorists or experimentalists. It, therefore, becomes especially important to adopt a different approach and attempt to study dynamical regime changes in our microplasma system, by performing a detailed study of its *microscopic* dynamics.

To this end, we shall focus hereafter on the lower energy range of Hamiltonian (5), where the transition from "crystalline–like" to "liquid–like" collective

behavior takes place. In the next section, we review the methods used for the detection of these dynamical regimes, i.e. the Smaller Alignment Index (SALI) [35, 37, 38] and the spectrum of Lyapunov exponents [7, 8] and compare the information provided by these approaches.

As we shall see, in the crossover regime, the SALI exhibits a rather intricate "stair–like" power law decay to zero, with different Lyapunov exponents, reminiscent of the "stickiness" behavior typically observed in the neighborhood of resonance islands of Hamiltonian systems [36]. In our case, this type of weakly chaotic dynamics will turn out to characterize the energy range over which the passage from ordered to irregular dynamics occurs, through what we call the "melting transition".

3 Methods for distinguishing between order and chaos

3.1 The Smaller Alignment Index (SALI)

The SALI method was initially introduced in [35] and has been applied successfully to distinguish between ordered and chaotic dynamics in maps of various dimensions [12, 11], in Hamiltonian systems [37, 38], as well as in problems of celestial mechanics [40, 41], galactic dynamics [28], field theory [19] and nonlinear 1–dimensional lattices [2, 3, 31].

Following [35], one considers the $2N$–dimensional phase space of an arbitrary autonomous Hamiltonian system

$$H(\vec{q},\vec{p}) \equiv H(q_1(t),\ldots,q_N(t),p_1(t),\ldots,p_N(t)) = E \tag{10}$$

where $\vec{q}$ is the canonical position vector, $\vec{p}$ is the corresponding canonical conjugate momentum vector and E is the total constant energy. The time evolution of an orbit of Hamiltonian (10) associated with an initial condition $\vec{x}(t_0) = (q_1(t_0),\ldots,q_N(t_0),p_1(t_0),\ldots,p_N(t_0))$ at time $t = t_0$ is defined as the solution of Hamilton's equations of motion

$$\frac{dq_i(t)}{dt} = \frac{\partial H}{\partial p_i(t)},\ \frac{dp_i(t)}{dt} = -\frac{\partial H}{\partial q_i(t)},\ i = 1,\ldots,N \tag{11}$$

and is called the orbit $\vec{x}(t)$ of eqs. (11) passing through $\vec{x}(t_0)$.

To define the Smaller Alignment Index (SALI), one uses the *variational equations*, which represent the linearization of Hamilton's equations of motion (11) about a reference orbit $\vec{x}(t)$ of the system and are defined as

$$\frac{d\vec{v_i}(t)}{dt} = \mathcal{J}(\vec{x}(t)) \cdot \vec{v_i}(t),\quad \forall i = 1,\ldots,2N \tag{12}$$

where $\mathcal{J}(\vec{x}(t))$ is the Jacobian of the right–hand side of eqs. (11) calculated about the orbit $\vec{x}(t)$. The vectors $\vec{v_i}(t), \forall i = 1,\ldots,2N$ are known as deviation vectors of the $\vec{x}(t)$. If we follow two of them, say $\vec{v_k}(t)$ and $\vec{v_l}(t)$, we can define the *Smaller Alignment Index* (SALI) as

$$\mathrm{SALI}(t) \equiv \min\left\{\left\|\frac{\vec{v_k}(t)}{\|\vec{v_k}(t)\|} - \frac{\vec{v_l}(t)}{\|\vec{v_l}(t)\|}\right\|,\ \left\|\frac{\vec{v_k}(t)}{\|\vec{v_k}(t)\|} + \frac{\vec{v_l}(t)}{\|\vec{v_l}(t)\|}\right\|\right\} \tag{13}$$

where $\|\cdot\|$ denotes the usual Euclidean norm defined in $\mathbb{R}^{2N}$.

If $\vec{x}(t)$ is chaotic then $\lim_{t\to\infty} \mathrm{SALI}(t) = \min\{0, 2\} = 0$ since both deviation vectors tend to align with the direction of the maximum Lyapunov exponent as t increases [38, 43]. Furthermore, it has been shown that the time evolution of the SALI for chaotic orbits tends to zero exponentially at a rate related to the difference of the two largest Lyapunov exponents λ_1 and λ_2 as [38]

$$\mathrm{SALI}(t) \propto e^{-(\lambda_1-\lambda_2)t}. \tag{14}$$

On the other hand, if the orbit is ordered, SALI exhibits small oscillations about a constant $\alpha \in (0, \sqrt{2}]$. This is so, because both deviation vectors tend to become tangential to the torus on which the orbit is evolving while remaining mutually linearly independent in time due the existence of local or global integrals of motion [37].

It follows that this sharply different behavior of the SALI for ordered and chaotic orbits makes it a reliable and computationally fast tool for distinguishing between order and chaos in Hamiltonian systems of any number of degrees of freedom. The choice of the initial deviation vectors is arbitrary and in general does not affect the method apart from some very special cases demonstrated theoretically and verified numerically in a number of previous works [35, 37, 38].

3.2 The spectrum of Lyapunov exponents

One of the most standard and well–established means for extracting information about the nature of a given orbit of a dynamical system is to calculate its maximum *Lyapunov Characteristic Exponent* (LCE) λ_1. If $\lambda_1 > 0$ the orbit is characterized as chaotic. The theory of Lyapunov exponents was first applied to characterize chaotic orbits by Oseledec [30], while the connection between Lyapunov exponents and exponential divergence of nearby orbits was given in [9, 32]. Benettin et al. [7, 8] studied the problem of the computation of all LCEs theoretically and proposed in [8] an algorithm for their efficient numerical evaluation. In particular, λ_1 is computed as the limit for $t \to \infty$ of the quantity

$$L_1(t) = \frac{1}{t} \ln \frac{\|\vec{v_1}(t)\|}{\|\vec{v_1}(0)\|}, \text{ i.e. } \lambda_1 = \lim_{t\to\infty} L_1(t) \tag{15}$$

where $\vec{v_1}(0)$, $\vec{v_1}(t)$ are deviation vectors from the orbit we want to characterize, at times $t = 0$ and $t > 0$ respectively. Similarly, all other LCEs, λ_2,λ_3,$\ldots$,λ_{2N} are computed as limits for $t \to \infty$ of analogous quantities, $L_2(t)$,$L_3(t)$,$\ldots$,$L_{2N}(t)$. In the present paper, we shall compute the values of all Lyapunov exponents (called the Lyapunov spectrum) using the algorithm proposed by Benettin et al. [7, 8].

Let us also recall that the Lyapunov spectrum of an N degree of freedom Hamiltonian system, i.e. $\{\lambda_i\}_{i=1}^{2N}$, exhibits a basic symmetry with $N-1$ of its members having the opposite sign of the other $N-1$ and two exponents, i.e. λ_N, λ_{N+1}, being equal to 0. So, the discussion from here on concerns only the positive half of the Lyapunov spectrum, $\{\lambda_i\}_{i=1}^{N-1}$ where $\lambda_i > 0$.

The calculation of the Lyapunov spectrum is computationally demanding, as its convergence often requires the integration of trajectories over very long time intervals. This convergence depends on the inverse of the largest Lyapunov

exponent or *Lyapunov time*. So, the closer λ_1 is to zero the longer the integration is needed to obtain reliable estimates for the full spectrum.

On the other hand, of particular importance to statistical mechanics is the connection of the sum of all positive Lyapunov exponents (an index of chaos based on microscopic quantities) to the Kolmogorov–Sinai entropy H_{KS} (a measure of disorder of a macroscopic nature), given by Pesin's celebrated theorem [32]

$$H_{KS} = \sum_{\lambda_i > 0} \lambda_i \tag{16}$$

in the case of zero escape rates. This connection has opened new directions in the applications of thermodynamics, using the underlying microscopic dynamics of chaotic orbits (for a review see [18, 21]).

4 Calculation of Lyapunov spectra

For the purposes of simplifying our analysis, let us consider the case of few ions, e.g. $N = 5$ and $\gamma = 0.07$ (i.e. a small system in a prolate trap). As mentioned above, in this setting, it is easier to detect dynamical regime changes, such as seen in Fig. 3, where we have plotted the Kolmogorov–Sinai entropy H_{KS} (see eq. (16)) as a function of the energy E of the microplasma Hamiltonian (5). Both H_{KS} and Lyapunov exponents grow less steeply than in the oblate case (quasi 2–dimensional trap) for the region of small energies, as already pointed out in [22].

This slow increase of H_{KS} and λ_i's exhibits an inflection point at low energies as is evident in the inset of Fig. 3. We remark that this inflection point occurs just above the energy threshold that permits ions to move around their fixed points, while beyond this energy we observe the transition from weak to strong chaotic behavior. Note that H_{KS} as well as the Lyapunov exponents exhibit a maximum around $E \approx 6.2$.

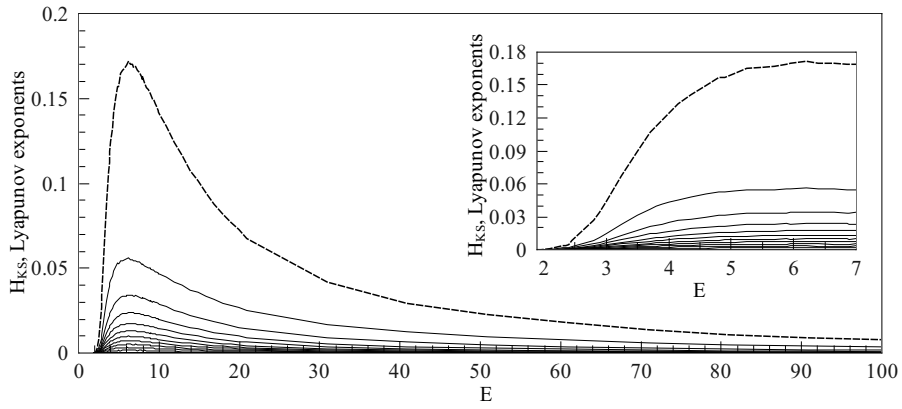

Figure 3: The Kolmogorov–Sinai entropy H_{KS}, for $\gamma = 0.07$ and $N = 5$, computed by the eq. (16) (dashed highest line) and the Lyapunov exponents (black solid lines) are plotted from the maximum down to the lowest one (15th) as a function of the energy. Note that, as shown in the inset, their maximum occurs at energies close to $E \approx 6.2$, which is much higher than the regime where the "melting transition" takes place (see text).

As a first attempt to derive useful information from the spectrum of Lyapunov exponents (see Fig. 3), in the energy range where the "melting transition" is expected to occur, we calculate the logarithms of the ratios of successive pairwise differences of Lyapunov exponents

$$\mathcal{P}_i(E) = \frac{\lambda_i - \lambda_{i+1}}{\lambda_{i+1} - \lambda_{i+2}},\ i = 1, \ldots, N-2,\ \lambda_i \equiv \lambda_i(E) \tag{17}$$

as a function of the energy (see Fig. 4). The calculation of all λ_i's was carried out for each trajectory up to a final integration time $t_f = 10^6$, ensuring that a relative convergence to 4 or 5 significant decimal digits has been achieved.

Note in Fig. 4(a) that the ratios (17) fluctuate wildly initially and only for $E \geq 2.3$ do they start to settle down to small oscillations about their ultimate values, which, at least for the first 2 or 3 ratios appear to be quite distinct. This suggests that it is within an interval $E_0 \lesssim E < 2.3$ where $E_0 \simeq 1.89$ that we should expect to find the "melting transition", where the positive Lyapunov exponents are very small, far from the values they attain in the regime of strong chaos (see inset of Fig. 3 for $E \geq 2.3$).

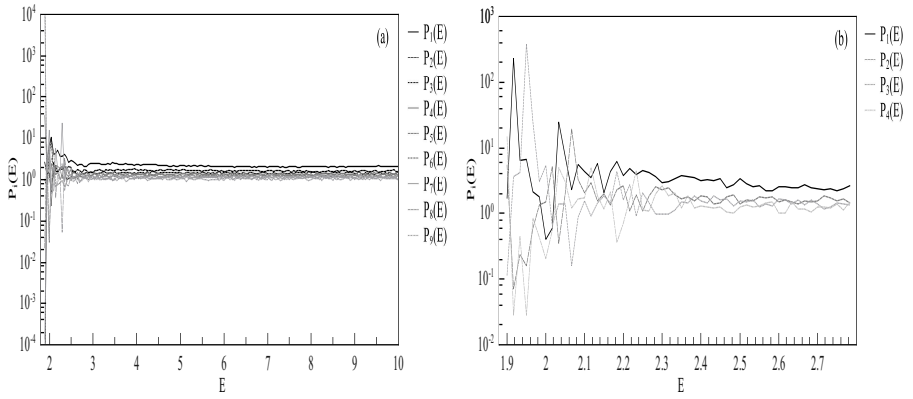

Figure 4: (a) Plot of the logarithms of the ratios $\mathcal{P}_i(E)$, $i = 1, \ldots, 9$ (see eq. (17)), for $\gamma = 0.07$ and $N = 5$, as a function of the energy E. Note the characteristic gaps in the spectrum appearing for large values of E. (b): Same as in panel (a) for $i = 1, \ldots, 4$ and small values of E, with the characteristic gaps in the spectrum becoming erratic in the regime of weak chaos, settling down to more clearly defined values around $E \geq 2.3$.

Undoubtedly, although the information concerning the existence of two distinct dynamical regimes at small energies is somehow contained in the plots of Fig. 4, expressions (17) still fail to provide a precise picture of this change. This is perhaps due to inaccuracies of the inherent averaging process used in the calculation of the $\mathcal{P}_i(E)$ at low energies, where the Lyapunov exponents are very small. We, therefore, proceed to study more carefully the underlying local microscopic dynamics by employing the SALI method we introduced previously.

5 Weak chaos detection

In this section, we apply the procedure outlined in Sec. 3.1 to analyze microscopically trajectories of the few–particle (i.e. $N = 5$ ions) microplasma system described by the Hamiltonian (5) in the prolate trap with $\gamma = 0.07$. We are thus able to identify at low energies a regime of weak chaos, through which the system passes from a "crystalline–like" type of ordered motion to the strongly chaotic behavior of collective soft modes. This is achieved by detecting qualitative changes in the SALI behavior for trajectories within the energy interval where the transition occurs.

Fig. 5 shows the behavior of the SALI as a function of time t at selected number of energies. These plots represent three distinct classes of long time behaviors for typical trajectories within the interval $1.9 \lesssim E \leq 3.5$. We have also computed, for the same sample of energies, the corresponding Lyapunov spectra for sufficiently long integration times (typically $t_f = 10^6$) to make sure that the Lyapunov exponents have converged to their limiting values up to a desired accuracy (typically to 4 or 5 significant decimal digits).

Fig. 5(a) represents the SALI evolution for a representative trajectory of system (5) at $E = 1.9$. We see that it fluctuates around non–zero positive

values up to an integration time of order $t_f = 10^6$, indicating that the motion (at least up to that time) is ordered and quasi-periodic. By contrast, in Fig. 5(b), we follow an orbit with energy $E = 3.5$ and find that SALI decays to zero exponentially fast, driven by the first gap in the Lyapunov spectrum of Fig. 4, according to the formula $e^{-(\lambda_1-\lambda_2)t}$ [38]. In this case, the first two Lyapunov exponents of the trajectory, $\lambda_1 \approx 0.03112$ and $\lambda_2 \approx 0.01746$, are large enough and distinct, implying strongly chaotic motion.

Finally, let us turn our attention to the intermediate and more interesting case where SALI exhibits a stair–like decay to zero as a function of time, at energies $2 < E < 2.3$ (see Fig. 5(c)). Choosing, for example, a trajectory with $E = 2.033$ we observe that SALI differs significantly compared to what is shown in Fig. 5(a) or 5(b). At first, one might think that, as in Fig. 5(a), the orbit is quasi-periodic, since SALI "sticks" to non–zero values for a fairly long time interval ($t \lesssim 4.4 \times 10^5$). Then, its behavior changes qualitatively, showing a near exponential decay to zero $\propto e^{-(\lambda_1-\lambda_2)t}$. This suggests that, even though the Lyapunov exponents (and their differences) are very small, eq. (14) still holds, as in the strongly chaotic domains of phase space [38].

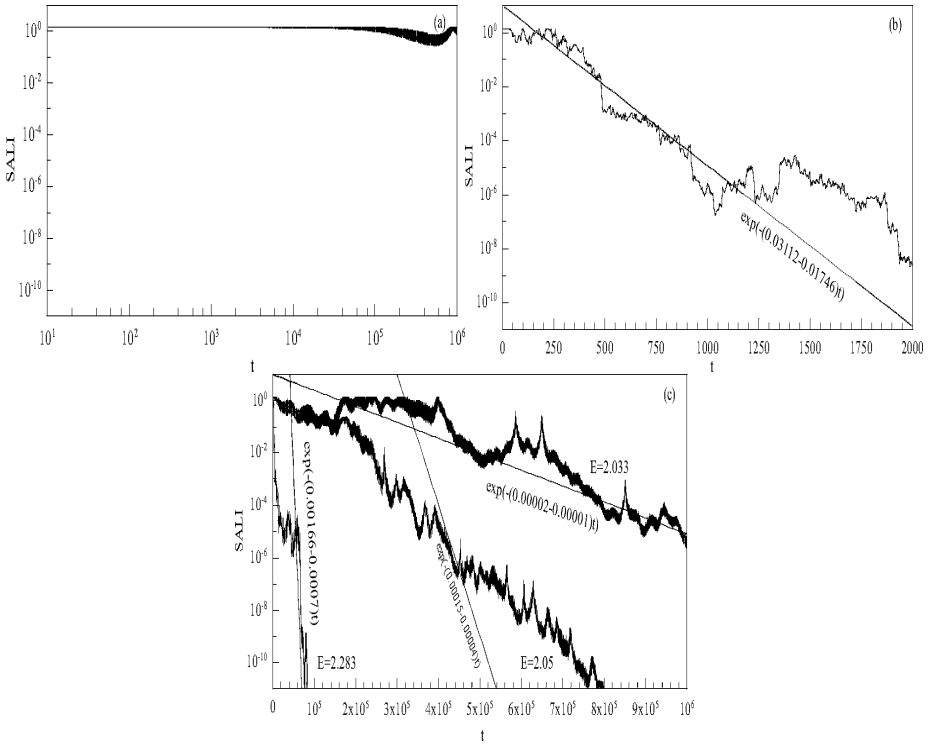

Figure 5: Plot of the evolution of SALI as a function of time t for $N = 5$, $\gamma = 0.07$ and 5 typical energies: (a) $E = 1.9$ where the motion is ordered. (b) $E = 3.5$ (strong chaotic behavior) where we also plot the theoretical prediction SALI$(t) \propto e^{-(\lambda_1-\lambda_2)t}$ for comparison. (c) $E = 2.033$, $E = 2.05$ and $E = 2.283$, plotting also the corresponding theoretical predictions. Note that all three vertical axes are logarithmic.

If we slightly increase the energy, however, to $E = 2.05$, SALI displays an intermediate and rather intricate behavior, following a stair–like decay to zero, shown by the middle curve in Fig. 5(c). Here, the exponential law (14) does not explain the SALI decay to zero. It appears that the motion lies within a weakly chaotic domain and "sticks" temporarily to islands of regular motion, executing a multi–stage diffusion process [36]. Finally, by increasing the energy to $E = 2.283$, we observe that SALI decays to zero exponentially fast, following closely the theoretical prediction $e^{-(\lambda_1-\lambda_2)t}$, with $\lambda_1 \approx 0.00166$ and $\lambda_2 \approx 0.0007$. These results imply that the corresponding trajectory is fully chaotic and the system has "melted", passing to a regime with strongly mixing properties.

We now examine more closely this step–wise decay of the SALI, observed in Fig. 5(c), over a range of energies spanning the melting transition. To this end, we start with our microplasma in the form of a Wigner crystal, at E_0 and proceed to the onset of thermal cloud formation, increasing the energy by steps of $\Delta E = 0.05$ up to $E_{max} = 6.2$.

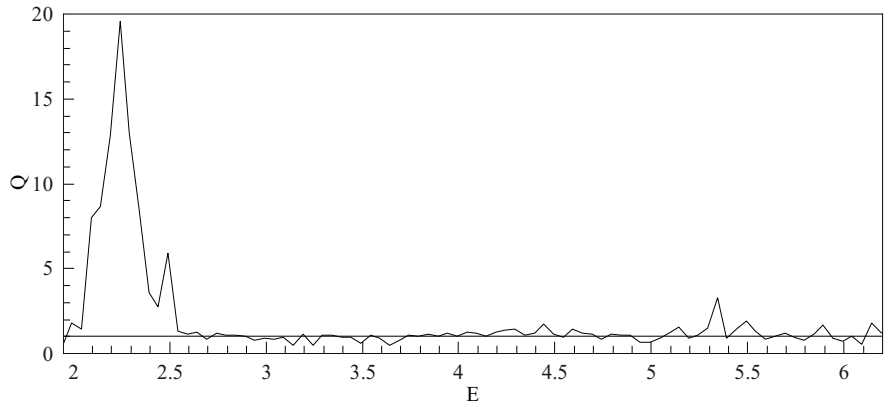

Figure 6: Plot of the quantity $Q = \frac{\Delta\lambda}{K}$, for $\gamma = 0.07$ and $N = 5$, as a function of the energy $E \in [E_0, E_{max}]$ where $\Delta\lambda$ is the difference of the two largest Lyapunov exponents and K is the slope calculated by linear regression performed on the log(SALI(t)) vs. t curves. We also plot the line $Q = 1$ to indicate the energy range where $\Delta\lambda = \lambda_1 - \lambda_2 \approx K$ and eq. (14) are satisfied.

One way to quantify the departure of the SALI from the exponential decay law (14) (see Fig. 5(c)) is to calculate for each energy in the interval $[E_0, E_{max}]$ the quantity

$$Q = \frac{\Delta\lambda}{K} \tag{18}$$

defined as the ratio of the difference between the two largest Lyapunov exponents $\Delta\lambda = \lambda_1 - \lambda_2$ and K, the linear regression estimate of this difference, obtained from semi–logarithmic plots of SALI, like those depicted in Fig. 5(b) and (c). The result is shown in Fig. 6. As expected, for the strongly chaotic cases where $K \approx \Delta\lambda$, we obtain values of Q near 1 with clearly negative log(SALI) slopes.

The interesting part of Fig. 6, however, is observed in the energy interval $2.0 < E < 2.5$ where K becomes one order of magnitude smaller than $\Delta\lambda$.

It is in this regime that we observe the "melting transition" for our system. The divergence of SALI from its theoretical estimate of eq. (14) signifies the presence of other collective modes of motion. This motion is organized around islands of stability, suggesting a certain type of "stickiness" around different tori at successive time intervals. During these time intervals SALI decays in a step–like manner by different power laws.

In fact, we can provide more evidence to support the above interpretation of the dynamics in the "melting phase", using a recent generalization of the SALI, called the *Generalized Alignment Indices* (GALI) [39]. These indices represent the volumes of a parallelepiped, called GALI_k, formed by $k \geq 2$ unit deviation vectors, which (a) for ordered motion, oscillate about positive constants as long as $k \leq d$ (d being the dimension of the torus) and decay following power laws for $k > d$, while (b) for chaotic orbits, they all vanish exponentially with exponents that become more negative as k increases and depend on more Lyapunov exponents [39, 36]. In practise, since the computation of the GALI requires the calculation of a fairly big number of large determinants at every time step, we have adopted an alternative way of evaluating it which is significantly faster in CPU time, the so called *Linear Dependence Index* (LDI) [1].

Thus, in Fig. 7, we use this approach to compute the GALI_k, $k = 2, \ldots, 10$ and find that they demonstrate the existence of an (at least 6–dimensional) torus for $E = 1.9$ [36], while they show a step–wise decrease for $E = 2$, which continues to hold up to $E \lesssim 2.283$, as predicted by the SALI ($= \mathrm{GALI}_2$) calculations (compare Fig. 5(a), (c) with Fig. 7(a) and (b)). Of course, as the energy increases, the (weakly) chaotic nature of the orbits becomes evident at earlier times (e.g. for $E = 2$ we have $t \approx 3 \times 10^6$ and for $E = 2.283$ we get $t \approx 6 \times 10^4$ for the LDI (or GALI) to become $\simeq 10^{-11}$) as we see in Fig. 7(b) and (c).

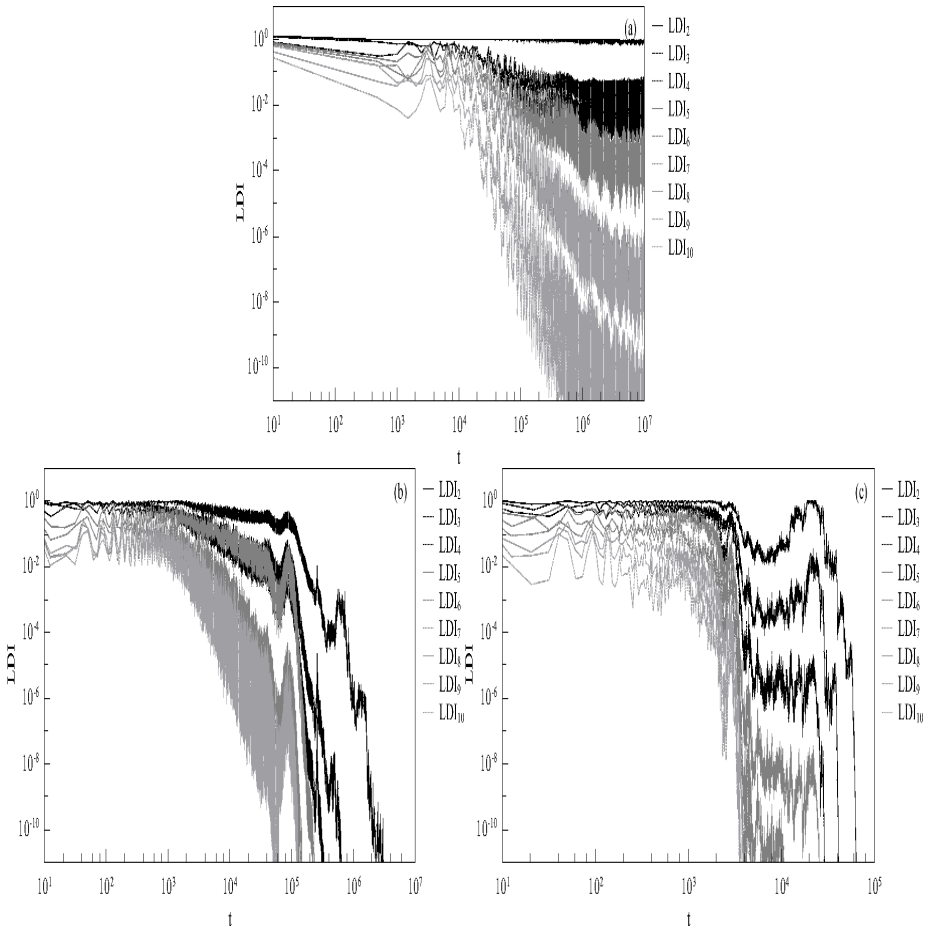

Figure 7: Plot of the LDI_k (=GALI_k), $k = 2, \ldots, 10$ as a function of time t for the microplasma system (5) of $N = 5$ ions in a prolate trap ($\gamma = 0.07$) for 3 typical energies. (a) LDI_2–LDI_{10} for the energy $E = 1.9$. (b) Same as in panel (a) for the slightly bigger energy $E = 2$. (c) Same as in panel (a) for the bigger energy $E = 2.283$. Note that all axes are logarithmic.

Thus, the above results suggest that the behavior of the SALI during dynamical regime changes is especially useful, as it alerts us to examine quantities like Q (see eq. (18)), related to variations in the differences of Lyapunov exponents. Such quantities indeed furnish important information, not readily available by other more standard microscopic chaotic indicators or by related macroscopic entropic quantities.

6 Conclusions

In this paper, we have reported results demonstrating the occurrence of dynamical regime changes in a Hamiltonian system describing a microplasma confined in a prolate quasi 1–dimensional configuration and characterized by long–range Coulomb interactions. More specifically, in the lower energy regime, we macro-

scopically detected the transition from "crystalline–like" to "liquid–like" behavior, through what we call the "melting phase". As expected, well beyond this phase, the microplasma exhibits strong chaotic behavior that may be described by the macroscopic variables of statistical mechanics. The question, therefore, is how can one determine the dynamical nature and identify the energy range of this "melting transition" from ordered to strongly chaotic behavior.

To this end, we first showed that the "melting" of our quasi 1–dimensional crystal (composed of few ions confined in a prolate trap) is not associated with a sharp increase of the temperature at some critical energy, as might have been expected. Furthermore, the positive Lyapunov exponents (and the Kolmogorov–Sinai entropy expressed by their sum) attain their highest values at energies much higher than the regime where the microplasma "melts". Thus, it appears that there is no clear "macroscopic" methodology for identifying and studying this "melting" process in detail.

Next, we argued that even though information about dynamical regime changes must be contained in the Lyapunov exponents, Lyapunov spectra by themselves still fail to provide, a more precise picture of this change. Indeed, while the ratios of the larger of them show strong fluctuations at low energies, these require further analysis before they can reveal, with any precision, the energies over which the "melting transition" occurs.

For these reasons, we found it useful to employ a more accurate tool, called the SALI method, to study in more detail the local microscopic dynamics of the microplasma system. In this way, we discovered an energy range of *weak chaos*, where the positive Lyapunov exponents are very small and SALI exhibits a stair–like decay to zero with varying decay rates. As $\mathrm{SALI}(t) \propto e^{-(\lambda_1-\lambda_2)t}$ in chaotic domains, this inspired us to look more closely at the statistical fluctuations of the differences of the two largest Lyapunov exponents $\Delta\lambda = \lambda_1 - \lambda_2$ in that regime. We, thus, observed that these differences exhibit their largest fluctuations over a definite energy interval, where "melting" occurs in a way reminiscent of "sticky" orbits, executing a multi–stage diffusion process near the boundaries of resonance islands in the phase space of Hamiltonian systems. The above results were also supported by the use of an extended set of indices which generalize SALI to the case of more than 2 deviation vectors.

Finally, we remark that it is also the rapid convergence of these indices, which turns them into efficient diagnostic tools that may be used to replace demanding molecular simulations in identifying weakly chaotic regimes in multi–particle systems. As we intend to show in a future publication, these indices can provide a viable alternative to the notoriously time consuming simulations required to study the presence of weak chaos and slow diffusive effects in the dynamics of metastable states.

7 Acknowledgements

The authors would like to thank professors G. Nicolis, P. Gaspard, G–L. Forti and Ch. Skokos as well as Dr. P. de Buyl for fruitful discussions, encouragement and support during the preparation of the paper. We would also like to thank the referees for their constructive remarks and suggestions. The work of Ch. A. was financially supported by the PAI 2007–2011 "NOSY–Nonlinear systems, stochastic processes and statistical mechanics" (FD9024CU1341) contract and

the work of V. B. by the Prodex program of the European Space Agency under contract No. ESA AO–2004–070 (C90241). The computer programs of this work were ran in the high–performance multiprocessor systems "PYTHIA" of ULB and "TURING" of UoP.

References

[1] Ch. Antonopoulos and T. C. Bountis. Detecting order and chaos by the Linear Dependence Index (LDI) method. *ROMAI Journal*, 2(2):1 – 13, 2006.

[2] Ch. Antonopoulos and T. C. Bountis. Stability of simple periodic orbits and chaos in a Fermi – Pasta – Ulam lattice. *Phys. Rev. E*, 73(1), 2006.

[3] Ch. Antonopoulos, T. C. Bountis, and Ch. Skokos. Chaotic dynamics of N – degree of freedom Hamiltonian systems. *Int. J. Bif. Ch.*, 16(6):1 – 18, 2006.

[4] D. M. Barnett and T. Tajima. Fluctuations and the many–body Lyapunov exponent. *Phys. Rev. E*, 54:6084 – 6092, 1996.

[5] D. M. Barnett, T. Tajima, K. Nishihara, and H. Furukawa. Lyapunov exponent of a many body system and its transport coefficients. *Phys. Rev. Lett.*, 76:1812 – 1815, 1996.

[6] M. Baus and C. F. Tejero. *Equilibrium statistical physics. Phases of matter and phase transitions.* Springer, 2008.

[7] G. Benettin, L. Galgani, A. Giorgilli, and J-M. Strelcyn. Lyapunov characteristic exponents for smooth dynamical systems and for Hamiltonian systems: A method for computing all of them. Part 1: Theory. *Meccanica*, 15:9 – 20, March 1980.

[8] G. Benettin, L. Galgani, A. Giorgilli, and J-M. Strelcyn. Lyapunov characteristic exponents for smooth dynamical systems and for Hamiltonian systems: A method for computing all of them. Part 2: Numerical application. *Meccanica*, 15:21 – 30, March 1980.

[9] G. Benettin, L. Galgani, and J-M. Strelcyn. Kolmogorov entropy and numerical experiments. *Phys. Rev. A*, 14:2338, 1976.

[10] R. Blümell, J. M. Chen, E. Peik, W. Quint, W. Schleich, Y. R. Shen, and H. Walther. Phase transitions of stored laser–cooled ions. *Nature (London)*, 334:309, 1988.

[11] T. Bountis and Ch. Skokos. Application of the SALI chaos detection method to accelerator mappings. *Nucl. Instr. and Meth. A*, 561:173 – 179, 2006.

[12] T. Bountis and Ch. Skokos. Space charges can significantly affect the dynamics of accelerator maps. *Phys. Let. A*, 358(2):126 – 133, 2006.

[13] L. R. Brewer, J. D. Prestage, J. J. Bollinger, W. M. Itano, D. J. Larson, and D. J. Wineland. Static properties of a non–neutral $^9Be^+$–ion plasma. *Phys. Rev. A*, 38:859, 1988.

[14] P. Butera and G. Caravati Phase transitions and Lyapunov characteristic exponents *Phys. Rev. A*, 36(2):962 – 964, 1987.

[15] L. Caiani, L. Casetti, C. Clementi and M. Pettini Geometry of Dynamics, Lyapunov Exponents, and Phase Transitions *Phys. Rev. Lett.*, 79(22):4361 – 4364, 1997.

[16] L. Casetti, M. Pettini and E. G. D. Cohen Geometric approach to Hamiltonian dynamics and statistical mechanics Physics Reports, 337(3):237 – 341, 2000.

[17] C. Casetti, M. Pettini, and E. G. D. Cohen. Phase transitions and topology changes in configuration space. *J. Stat. Phys.*, 111(516):1091 – 1123, 2003.

[18] P. Cvitanović, R. Artuso, R. Mainieri, G. Tanner, and G. Vattay. *Chaos: classical and quantum.* `ChaosBook.org`, Niels Bohr Institute, Copenhagen, 2009.

[19] L. P. G. de Assis, J. A. Helayel Neto, F. Haas, and A. L. M. A. Nogueira. On the integrability and chaos of an $N = 2$ Maxwell–Chern–Simons–Higgs mechanical model. *PoS*, IC2006:059, 2006.

[20] M. C. Firpo. Analytic estimation of the Lyapunov exponent in a mean–field model undergoing a phase transition. *Phys. Rev. E*, 57:6599, 1998.

[21] P. Gaspard. *Chaos, scattering and statistical mechanics.* Cambridge University Press, 1998.

[22] P. Gaspard. Lyapunov exponent of ion motion in microplasmas. *Phys. Rev. E*, 68(056209):1 – 7, 2003.

[23] T. L. Hill. *Statistical mechanics.* Dover, New York, 1987.

[24] T. L. Hill. *Thermodynamics of small systems.* Dover, New York, 1994.

[25] J. Hoffnagle and R. G. Brewer. Frequency–locked motion of two particles in a Paul trap. *Phys. Rev. Lett.*, 71:1828, 1993.

[26] J. Hoffnagle, R. G. DeVoe, L. Reyna, and R. G. Brewer. Order–chaos transition of two trapped ions. *Phys. Rev. Lett.*, 61:255, 1988.

[27] V. Latora, A. Rapisarda, and S. Ruffo. Lyapunov instability and finite size effects in a system with long–range forces. *Phys. Rev. Lett.*, 80:692, 1998.

[28] T. Manos, Ch. Skokos, E. Athanassoula, and T. Bountis. Studying the global dynamics of conservative dynamical systems using the SALI chaos detection method. *Nonlinear Phenomena in Complex Systems*, 11(2):171 – 176, 2006.

[29] V. Mehra and R. Ramaswamy, Ramakrishna Curvature fluctuations and the Lyapunov exponent at melting *Phys. Rev. E*, 56(3):2508 – 2517, 1997.

[30] V. I. Oseledec. A multiplicative ergodic theorem: Lyapunov characteristic numbers for dynamical systems. *Trans. Moscow Math. Soc.*, 19:197 – 231, 1968.

[31] P. Panagopoulos, T. Bountis, and Ch. Skokos. Existence and stability of localized oscillations in 1 – dimensional lattices with soft spring and hard spring potentials. *J. Vib. Acc.*, 126:520 – 527, 2004.

[32] Y. B. Pesin. Characteristic Lyapunov exponents and smooth ergodic theory. *Rus. Math. Sur.*, 32:55 – 114, 1977.

[33] M. G. Raizen, J. M. Gilligan, J. C. Bergquist, W. M. Itano, and D. J. Wineland. Ionic crystals in a linear Paul trap. *Phys. Rev. A*, 45:6493, 1992.

[34] I. Siemers, R. Blatt, Th. Sauter, and W. Neuhauser. Dynamics of ion clouds in Paul traps. *Phys. Rev. A*, 38:5121, 1988.

[35] Ch. Skokos. Alignment Indices: A new, simple method for determining the ordered or chaotic nature of orbits. *J. Phys. A: Math. & Gen.*, 34:10029 – 10043, 2001.

[36] Ch. Skokos, Ch. Antonopoulos, and T. C. Bountis. Detecting chaos, determining the dimensions of tori and predicting slow diffusion in Fermi – Pasta – Ulam lattices by the Generalized Alignment Index method. *Eur. Phys. J. Special Topics*, 165:5 – 14, 2008.

[37] Ch. Skokos, Ch. Antonopoulos, T. C. Bountis, and M. N. Vrahatis. How does the Smaller Alignment Index (SALI) distinguish order from chaos? *Prog. Theor. Phys. Sup.*, 150:439 – 443, 2003.

[38] Ch. Skokos, Ch. Antonopoulos, T. C. Bountis, and M. N. Vrahatis. Detecting order and chaos in Hamiltonian systems by the SALI method. *J. Phys. A: Math. & Gen.*, 37:6269 – 6284, 2004.

[39] Ch. Skokos, T. C. Bountis, and Ch. Antonopoulos. Geometrical properties of local dynamics in Hamiltonian systems: The Generalized Alignment Index (GALI) method. *Physica D*, 231:30 – 54, 2007.

[40] A. Széll. *Investigation of the Caledonian symmetrical four – body problem.* PhD thesis, Glasgow Caledonian University, 2003.

[41] A. Széll, B. Érdi, Zs. Sándor, and B. Steves. Chaotic and stable behaviour in the Caledonian symmetric four – body problem. *Monthly Notices of the Royal Astronomical Society*, 347:380 – 388, 2004.

[42] Y. Ueshima, K. Nishihara, D. M. Barnett, and H. Furukawa. Particle simulation of Lyapunov exponents in one–component strongly coupled plasmas. *Phys. Rev. E*, 55:3439, 1997.

[43] N. Voglis, G. Contopoulos, and C. Efthymiopoulos. Detection of ordered and chaotic motion using the dynamical spectra. *Cel. Mec. Dyn. Astr.*, 73:211 – 220, 1999.

[44] C. Yannouleas and U. Landman. Symmetry breaking and quantum correlations in finite systems: Studies of quantum dots and ultracold bose gases and related nuclear and chemical methods. *Reports on Progress in Physics*, 70(12):2067 – 2148, 2007.